

Dear Editor,

Thanks for the kind comments to this revised manuscript, and we have further revised the manuscript based on the comment of Minor Revise. More detail please see below:

Comment---Minor Revise

both reviewers identified requires further attention - the introduction. Reviewer 1 suggests re-writing the introduction - and the track changes for section indicate there are a few but not substantial changes here. Reviewer 2 also asks for a greater overview in the introduction - of which changes have been made in section 2 (study area not introduction) and in the supplemental material.

Therefore - before publication - I request that you revise the introduction - possibly combine it with the study area section (section 2) and provide a clearer context for the work. For the non specialist in the area (and ESURFs readership may be interested but not know all the details of the area and the issues) at present it is not completely clear what the issue you need to investigate is. So please - in the introduction - make sure you cover firstly what the research issue to be addressed is - what the knowledge gap lies. How previous studies have addressed this - and left the issue to be addressed - and finally how this paper aims to address those issues.

**Answer:** We have revise the Introduction, combined the Introduction with section 2 of The study area following the comment, and further revise were carried out, in order to let the Introduction can cover the what the research issue to be addressed is - what the knowledge gap lies. How previous studies have addressed this - and left the issue to be addressed - and finally how this paper aims to address those issues. Please see Introduction section.

Moreover, following the comments, the co-author's affiliations were checked and revised.

---

# Holocene sea-level change on the central coast of Bohai Bay, China

Fu Wang<sup>1,2</sup>, Yongqiang Zong<sup>3</sup>, Barbara Mauz<sup>4,5</sup>, Jianfen Li<sup>1,2</sup>, Jing Fang<sup>6</sup>, Lizhu Tian<sup>1,2</sup>, Yongsheng Chen<sup>1,2</sup>, Zhiwen Shang<sup>1,2</sup>, Xingyu Jiang<sup>1,2</sup>, Giorgio Spada<sup>7</sup> and Daniele Melini<sup>8</sup>

<sup>1</sup>Tianjin Center ~~of Geological Survey~~, China Geological Survey (CGS), Tianjin, China

<sup>2</sup>Key Laboratory of Coast Geo-Environment, China Geological Survey, CGS, Tianjin, China

<sup>3</sup>Department of Earth Sciences, The University of Hong Kong, Hong Kong SAR, China

<sup>4</sup>School of Environmental Sciences, University of Liverpool, Liverpool, UK

<sup>5</sup>Department of Geography and Geology, University of Salzburg, Salzburg, Austria

<sup>6</sup>~~College of Urban~~School of Geography and Environmental Sciences, Tianjin Normal University, Tianjin, China

<sup>7</sup>Department of Science, University of Urbino, Urbino, Italy

<sup>8</sup>Istituto Nazionale di Geofisica e Vulcanologia, Roma, Italy

*Correspondence to: Fu Wang (wfu@cgs.cn)*

Abstract. To constrain models on global sea-level change regional proxy data on coastal change are indispensable. Here, we reconstruct the Holocene sea-level history of the northernmost China Sea shelf. This region is of great interest owing to its apparent far-field position during the late Quaternary, its broad shelf and its enormous sediment load supplied by the Yellow River. This study generated 25 sea-level index points for the central Bohai coastal plain through the study of 15 sediment cores and their sedimentary facies, foraminiferal assemblages and radiocarbon dating the basal peat. The observational data were compared with sea-level predictions obtained from global GIA models and with published sea-level data from Sunda shelf, Tahiti and Barbados. Our observational data indicate a phase of rapid sea-level rise from c. -17 m to -4 m between c. 10 ka and 5 ka with a peak rise of 6.4 mm/a during 8.7 ka to 7.5 ka and slower rise of 1.9 mm/a during 7.5 ka to 5.3 ka followed by a phase of slow rise from 5 ka to 2 ka (~0.4 mm/a from -3.58 m of 5.3 ka cal BP to -2.15 m of 2.3 ka cal BP). The comparison with the sea-level predictions for the study area and the published sea-level data is insightful: in the early Holocene Bohai Bay's sea-level rise is dominated by a

29 combination of the eustatic and the water load components causing the levering of the broad shelf. In the mid-  
30 late Holocene the rise is dominated by a combination of tectonic subsidence and fluvial sediment load which  
31 masks the mid-Holocene highstand recorded elsewhere in the region.

32

33

34 KEYWORDS: Sea level; Holocene; Glacial Isostatic Adjustment; Ice Equivalent Sea Level; Bohai Bay

### 35 1. Introduction

36 The sea-level rise since the mid-19th century is one of the major challenges to humanity of the 21st century  
37 (IPCC, 2014). The driving mechanisms of this rise are relatively well-known on a global scale, but on a regional  
38 scale the mechanisms are modified by ~~local parameters. One of these parameters is the~~ regional Holocene sea-  
39 level history, ~~which~~This history is a background ~~sea level~~ signal controlled by ice load and corresponding  
40 response of the the deformable Earth (Clark et al., 1978) and, in addition, by regional parameters such as fluvial  
41 sediment supply and shelf geometry. of variable amplitude. In fact, the regional response to sea-level changes  
42 may be very different from the global signal (Nicholls and Cazenave, 2010), and, understanding regional costal  
43 environment is a rising demand of policy makers.

44 Here, we study the Holocene sea-level history of Bohai Sea, which is the northernmost part of China Sea (Fig.  
45 1) and situated ~~The area is of special interest because its shoreline is situated on the broad shelf of the East~~  
46 ~~China Sea (Fig. 1)~~ in the far-field of the former ice sheets. The area is of special interest because its receives a  
47 large amount of fine-grained Yellow River sediment and because its shoreline is situated on the broad shelf of  
48 the East China Sea (Fig. 1). During the Holocene sea-level rise the increasing water load in the west Pacific  
49 Ocean basin should have lifted the Bohai Sea shelf and push the shoreline landward while the fluvial sediment  
50 input should have pushed the shoreline seaward. The two processes may have peaked at different times and  
51 their contrasting effect on shoreline migration may have varied accordingly. Beyond that, being situated in the  
52 far-field, the shoreline should have migrated landward in response to the rising water level. The shelf effect  
53 and the rising water level is well-described by sea-level physics and the associated glacio-isostatic adjustment

(GIA) models predict a ~~While the far field site should have a sea level history similar to the ice equivalent sea level, the broad shelf is thought to affect the~~ sea-level ~~elevated~~ by up to 10 m height ~~due to shelf levering~~ (e.g. Milne and Mitrovica, 2008). ~~Indeed, a several meter sea-level highstand is predicted for the East China Sea coast during the mid-Holocene (Bradley et al., 2016) but this high highstand seems to be an overestimate when compared to observational data (Bradley et al., 2016) which indicate in a spatially complex manner. For example, only a very minor Holocene highstand was recorded at sites along the southeast and south coast of the East China Sea coast (Zong, 2004).~~ ~~In fact, and~~ no obvious Holocene highstand ~~for delta area of~~ ~~was recorded in the Hangzhou Bay Yangtze River~~ (Xiong et al., 2020) and the Pearl River delta (Xiong et al., 2018). ~~From this the question arises, if the observational data are inaccurate, if the GIA model parameters are too poorly constrained and how fluvial sediment supply influences the sea-level history.~~

~~In our study area, observational data were firstly obtained from chenier ridges (Wang, 1964). Subsequently, a series of studies on marine transgression and lithostratigraphy provided the framework for understanding the late Quaternary evolution of Bohai Bay (e.g., Zhao et al., 1979; Fig. S1) and, over time, over 130 Holocene sea-level data, generated in the study area since the early 60ths, were recently compiled by Li et al. (2015; Fig. S2; for details see supplement). However, because no correction for compaction was carried out, uncertainties were poorly constrained and no screening took place by which unsuitable material (e.g., transported shell) is rejected, the dataset requires further scrutiny and is not used in our study. Instead~~ ~~In addition, the exceptionally high supply of fine grained fluvial sediment to the bay should have influenced shoreline migration in the past.~~

~~In order to reliably constrain the~~ ~~we established new~~ sea-level ~~data based on saltmarsh peat or peaty clay collected from drilling cores~~ ~~history in such complex settings, high resolution proxy data are required and~~ compared with glacio-isostatic adjustment (GIA) model predictions. ~~where~~ ~~†~~ ~~The~~ difference between model and ~~proxy datum~~ ~~observational datum~~ should allow inferring the non-GIA, hence ~~fluvial~~ ~~local~~, impact on the sea-level history. We show here that shelf effect and local processes influence the regional sea-level history at different times.

## 78 2. The study area

79 The study area lies in a mid-latitude, temperate climate zone (Fig. 1a) on the north-western coast of the East  
80 China Sea's wide shelf. Geologically, the Bohai Bay is a depression filled by several kilometre-thick  
81 Cenozoic sediment sequences with the top 500 m ascribed to the Quaternary (Wang and Li, 1983). The long-  
82 term tectonic subsidence has been estimated to about 1.3-2.0 mm/a at Tianjin City (Wang et al., 2003). The  
83 Bay is a semi-enclosed marine environment, connected to the Pacific through a gap between the two  
84 peninsulas, Liaodong Peninsulas and Shangdong Peninsulas and the Yellow Sea (Fig. 1b). Our study area is  
85 the central coast of the Bay which lies between two deltaic plains, the Yellow River delta in the south and the  
86 Luan River delta in the north (Fig. 1b). Several small rivers (e.g., Haihe and Duliujianhe, Fig. 1c) cut through  
87 the coastal plain and enter the Bay. The coastal lowland is characterised not only by its low-lying nature,  
88 (less than 10 m above sea level), but also by a series of chenier ridges situated south of the Haihe River and  
89 buried oyster reefs situated north of the Haihe River (Fig. 1c; Li et al., 2007; Su et al., 2011; Wang et al.,  
90 2011; Qin et al., 2017). Local reference tidal levels such as mean high waters (MHW) and highest high  
91 waters (HHW) are 1.25 m and 2.30 m respectively, based on the four tidal stations on the coast of Bohai Bay  
92 (Fig. 1c). During the Last Glacial Maximum the shoreline moved to the shelf break of the Yellow Sea, more  
93 than 1000 km to the east and southeast of our study area (e.g., He, 2006). During the Holocene the sea  
94 inundated the coastal area with the shoreline moving about 80 km inland (e.g., Wang et al., 2015).

95 ~~Previous studies focused on the chenier ridges and palaeo-shoreline change of Bohai Bay (Wang, 1964).~~  
96 ~~Subsequently, a series of studies on marine transgression and lithostratigraphy provided the framework for~~  
97 ~~understanding the late Quaternary evolution of Bohai Bay (e.g., Zhao et al., 1979; Fig. S1). Over 130 Holocene~~  
98 ~~sea level data, generated in the study area since the early 60ths, were recently compiled by Li et al. (2015; Fig-~~  
99 ~~S2; for details see supplement). However, because no correction for compaction was carried out and no~~  
100 ~~screening took place by which unsuitable material (e.g., transported shell) is rejected, the dataset requires~~  
101 ~~further scrutiny and is not used in our study.~~

## 102 3 Methods

---

### 103 3.1 Sampling and elevation measurements

104 To obtain sedimentary sequences for this study, we consulted previous studies (*e.g.* Cang *et al.*, 1979; Geng,  
105 1981; Wang *et al.*, 1981; Wang, 1982; Yang and Chen, 1985; Zhang *et al.*, 1989; Zhao *et al.*, 1978; Xue *et*  
106 *al.*, 1993) to learn where in the bay marine deposits are dominant and where the landward limit of the last  
107 marine transgression should occur. We then collected 15 cores along W-E transects from the modern  
108 shoreline to 80 km inland (Fig. 1c), using a rotary drilling corer. Transect A, comprising 6 cores, stretches  
109 from the modern shoreline 80 km inland and crosses the inferred Holocene transgression limit (Xue, 1993).  
110 Transects B, C and D, comprising 9 cores, cross the transgression limit a little further south (Fig. 1c). The  
111 surface elevations of the drilled cores were levelled to the National Yellow Sea 85 datum (or mean sea level,  
112 MSL) using a GPS-RTK system with a precision of 3 cm. The GPS-RTK raw data were corrected and  
113 processed to National Yellow Sea 85 datum system by the CORS system network available from the Hebei  
114 Institute of Surveying and Mapping with National measurement qualification.

### 115 3.2 Sediment and peat analyses

116 In the laboratory, the sediment cores were opened, photographed and recorded for sedimentary characteristics  
117 including grain size, colour, physical sedimentary structures, and content of organic material. To study the  
118 degree of marine influence in the muddy sediment sequences, sub-samples were collected in 20 cm intervals.  
119 These were analysed with respect to diatoms and foraminifera with a subsequent focus on the foraminifera  
120 due to poor preservation of diatoms. The foraminifera of the >63 $\mu$ m fraction of 20 g dry sample were  
121 counted (*e.g.*, Wang *et al.*, 1985) following studies on modern foraminifera (*e.g.* Li, 1985; Li *et al.*, 2009).  
122 Sediment description followed Shennan *et al.* (2015): where in the sediment sequences foraminifera first  
123 appear and/or significantly increase (from zero or less than 10 to more than 50) is noted as transgressive  
124 contact, while the sediment horizon where foraminifera disappear and/or decrease significantly are noted as  
125 regressive contact. These changes are often associated with lithological changes, such as from salt-marsh  
126 peaty sediment to estuarine sandy sediment or tidal muddy sediment across a transgressive contact, or vice

127 versa. In addition, peat material was analysed in terms of its foraminifera content so that salt-marsh peat can  
128 be differentiated from freshwater peat.

### 129 **3.3 Analysis of compaction**

130 Because the Holocene marine deposits are mainly unconsolidated clayey silt with around 0.74% organic  
131 matter (Wang et al. 2015) post-depositional auto-compaction (Brain et al., 2015) may have led to lowering of  
132 the SLIP. According to Feng et al. (1999), the water content and compaction of marine sediments show  
133 positive correlation with the down-core reduction of water content of the Holocene marine sediment being  
134 about 10%. Based on these observations, we assumed the maximum lowering is about 10% of the total  
135 thickness of the compressible sediment beneath each SLIP. Consequently, the total lowering for an affected  
136 SLIP is 10% of the total thickness of the compressible sequence beneath the dated layer divided by the post-  
137 depositional lapse time proportional to the past 9000 years (e.g. Xiong et al., 2018), i.e. since the marine  
138 transgression in the study area.

### 139 **3.4 Radiocarbon analyses**

140 69 bulk organic sediment samples from salt-marsh peat were collected from drilling cores, and the peat or  
141 plant subsamples obtained from these bulk sediments were chosen for AMS radiocarbon analysis at Beta  
142 Analytic Inc. because these can give more reliable ages than shells for the SLIPs. The resulting raw  
143 radiocarbon ages were converted to conventional ages after isotopic fractionation were corrected based on  
144  $\delta^{13}\text{C}$  results. The conventional radiocarbon ages were calibrated to calendar years using the data set Intcal13  
145 included in the software Calib Rev 7.0.2 for organic samples, peat and plant samples (Reimer, *et al.*, 2013).  
146 Because Shang et al. (2018) reported age overestimation of 467 years for the bulk organic fraction of salt-  
147 marsh peaty clay compared to the corresponding peat fraction, all the AMS  $^{14}\text{C}$  ages between 4000 to 9000  
148 BP obtained from salt-marsh samples were corrected by  $Y=0.99X-466.5$  ( $Y$  is the corrected age,  $X$  is the age  
149 obtained from the organic fractions; Shang et al., 2018) except one <600 years age from borehole Q7 (Table  
150 1).

---

### 151 3.5 Sea-level index points (SLIPs)

152 To develop SLIPs, salt-marsh peaty clay layers were used. To convert the dated peat layers into a SLIP, the  
153 modern analogue approach was used by measuring the elevation of the modern open tidal flat (Fig. 2) and  
154 sampling its surface for their foraminiferal content. Following the studies of the modern foraminifera  
155 assemblage (Li, 2009) *Ammonia beccarii* typically occurs in the upper part of an intertidal zone and  
156 *Elphidium simplex* in the lower intertidal zone. The zonation of the modern foraminifera assemblage was  
157 then used to identify the indicative meaning of the salt-marsh peat layers: the paleo-mean sea level is the  
158 midpoint between high water of spring tides (HHW:+2.3 m) and mean high waters (MHW:+1.25 m) which is  
159 1.78 m with  $\pm 0.53$  m uncertainty (Wang et al., 2012, 2013; Li et al., 2015). For each dated salt-marsh peat  
160 layer the indicative meaning and range, the total amount of possible lowering in elevation due to sediment  
161 compaction and the reconstructed elevation of palaeo-MSL are listed in Table 1.

### 162 3.6 GIA modelling

163 The time-evolution of sea level was obtained using the open source program SELEN (Spada and Stocchi,  
164 2007) to solve the "Sea Level Equation" (SLE) in the standard form proposed in the seminal work of Farrell  
165 and Clark (1976). In its most recent development, SELEN (version 4) solves a generalized SLE that accounts  
166 for the horizontal migration of the shoreline in response to sea-level rise, for the transition from grounded to  
167 floating ice and for Earth's rotational feedback on sea level (Spada and Melini, 2019). The programme  
168 combines the two basic elements of GIA modelling (Earth's rheological profile and ice melting history since  
169 the Last Glacial Maximum) assuming a Maxwell viscoelastic incompressible rheology. The GIA models  
170 adopted are ICE-5G(VM2) (Peltier et al., 2004), ICE-6G(VM5a) (Peltier et al., 2012), both available on the  
171 home page of WR Peltier, and the one developed by Kurt Lambeck and colleagues (National Australian  
172 University, denoted as ANU hereafter; Nakada and Lambeck, 1987, Lambeck et al., 2003) provided to us by  
173 A Purcell (pers. com. 2016). Table S1 summarises the values used for each model. The palaeo-topography  
174 has been solved iteratively, using the present-day global relief given by model ETOPO1 (Amante and Eakins,  
175 2009). All the fields have been expanded to harmonic degree 512, on an equal-area icosahedron-based grid  
176 (Tegmark, 1996) with a uniform resolution of  $\sim 20$  km. The rotational effect on sea-level change has been  
177 taken into account by adopting the "revised rotational theory" (Mitrovica and Wahr, 2011).



---

## 178 4. Results

### 179 4.1 Lithostratigraphy and facies

180 Lithostratigraphically, the cores show a succession of terrigenous (including fresh-water swamp, river  
181 channel, flood plain), salt marsh and marine sediments (Table S2) with a clear W-E trend from terrestrial to  
182 marine dominance of deposits (Fig. 3-6). The around 80 km long transect A shows this trend: close to the  
183 modern shoreline pre-Holocene terrigenous sediments are overlain by basal peat including salt-marsh peat or  
184 peaty clay. Further inland these are replaced by fresh-water peat overlain by salt marsh and intertidal  
185 sediments and, above, by terrigenous sediments. The cores DC01, CZ01 and CZ02 are composed of fluvial  
186 sediments only, roughly confirming the Holocene maximum transgression inferred by Xue (1993). Multiple  
187 shifts between salt marsh, marine and fluvial deposits are noticeable in cores QX02, QX03, CZ61 which  
188 originate from the central part of the study area.

189 Marsh deposits are either a blackish and thin freshwater peat mostly interbedded in yellowish fluvial  
190 sediments or a yellowish-brown salt-marsh peat bearing intertidal foraminifera (Table 1). Their lower  
191 boundaries are usually sharp, and their upper boundaries are mostly diffused or the salt-marsh peat changes  
192 gradually into dark grey intertidal sediments. Salt-marsh peat is intercalated in marine sediment sequences  
193 (i.e. QX01, QX02, CZ61, CZ85, CZ66 and CZ03, Fig. 3-6), particularly at sites that are close to the  
194 Holocene maximum transgression limit.

### 195 4.2 Foraminifera data

196 Foraminifera were identified in all cores except CZ01, CZ02 and DC01 which originate from the landward  
197 site of the maximum transgression limit. As the Fig. 4 and 6 show that, foraminifera start to appear at 11.2 m  
198 depth, which is dated to about 7.85 ka cal BP in QX01. Abundance of fossil foraminifera changes from about  
199 404 – 772 individuals per samples at depths from 11.2 m to 10.8 m, 68 – 338 specimens from 9.4 m to 8.8 m,  
200 and 103 – 3456 counts from 8.2 m to 7.6 m. The assemblages reach maximum abundance at 6.6 m depth  
201 which is dated to between 5.29 and 5.23 ka cal BP, with over 30,000 individuals per sample, before  
202 disappearing at 5.6 m. Dominant species change from *Nonion glabrum* in 11.2 – 7.4 m to *Ammonia beccarii*  
203 vars. in 7.4 – 6.4 m. This change represents a change from a salt marsh to a lagoon. In QX02, the pattern of

204 foraminifera distributions is very similar. Low numbers of foraminifera, mostly *Nonion glabrum*, start to  
205 appear at about 10.1 m (-6.53 m of sea level), as dated to between 7.87 and 7.49 ka cal BP. The abundance  
206 reaches its highest at 6.7 m (-3.13 m of sea level), and the assemblages were dominated by *Ammonia beccarii*  
207 vars. Foraminifera disappears sometime between 5.72 and 3.52 ka cal BP. In all seaward drilling core, CZ03,  
208 CZ80, CZ85, CZ66, CZ87, CZ61, CZ65, ZW15 and Q7, the pattern of foraminifer's distributions are very  
209 similar as QX01 and QX02 (Fig. 4). The foraminifera start to appear in low numbers in the layer just above  
210 the basal peaty clay. This first appearance is in ca. 17-8 m depth dated to 9-7 ka cal BP. Above this depth the  
211 count increases from ~100 to ~3000 foraminifera per sample at ca 8-7 m depth. The maximum count  
212 with >30,000 individuals per sample is reached at -6-5 m dated to around 5 ka cal BP. Foraminifera  
213 disappear in these cores sometime between 5.7 ka cal BP and 3.5 ka cal BP. The foraminifera assemblage is  
214 composed of few species only, hence not rich and first dominated by *Nonion glabrum* in 17-7 m depth and  
215 then dominated by *Ammonia beccarii* vars. in 7-6 m depth. Other species found are *Quinqueloculina*  
216 *akneriana rotunda* and *Protelphidium tuberculatum* (Figs. 4 and 6).

#### 217 4.3 Modern analogue and indicative meaning and range

218 The data obtained from the modern analogue shows that the tidal flat can be divided into two sub-  
219 environments: intertidal with bioturbation (worm hole developed in tidal surface) and supratidal with salt-  
220 marsh vegetation (Fig. 2). Within the supratidal and salt-marsh zones, the foraminiferal assemblages are  
221 dominated by *Ammonia beccarii* covering an elevation range from +1.42 m to +2.00 m, including the +1.79m  
222 boundary of salt marsh with plants. At sites below these elevations, i.e. intertidal with bioturbation (Fig. 2),  
223 the foraminiferal assemblages are dominated by *Elphidium simplex*, *Ammonia beccarii* and *Pseudogyroidina*  
224 *Sinensis*. This foraminiferal zone covers an elevation ranging from 1.42 m to modern MSL.

225 Besides occasional *A. beccarii* there are few living foraminifera in the salt marsh above the MHW. The  
226 abundance is either biased towards *Ammonia beccarii* or it is relatively small. The latter is most probably due  
227 to the area being situated above the MHW and, hence, subject to evaporation during low tide, with the  
228 consequence of a relatively high and highly variable salt content of the pore water in the intertidal zone. The  
229 modern analogue samples confirm the bias towards salt-tolerant species (Fig. 2, Table 1). The spatial

230 distribution of the ages confirms the E-W trend of the Holocene transgression where the oldest age is close to  
231 the modern shoreline and the youngest age is close to the maximum transgression limit.

#### 232 **4.4 Sea-Level Index Points**

233 In total 25 sea-level index points were established from the dated basal salt-marsh peat using the information  
234 obtained from the modern analogue. In Core Q7, at the most seaward location in the study area, the basal  
235 SLIP is dated to ~9700 cal BP (Table 1), marking the onset of marine inundation of the study area. The  
236 overlying marine sequence is capped by a thick layer of shelly gravels at 1.30 m depth and the associated  
237 SLIP is dated to 540 cal BP. This marks the upper end of the marine sequence as foraminifera start to  
238 disappear alongside a change from intertidal to supratidal environmental conditions. The cores ZW15, QX02,  
239 QX03, QX01 show the same sequence as Q7 and provide 6 SLIPs. 19 SLIPs were collected from other cores  
240 (Table 1).

### 241 **3. Discussion**

#### 242 **5.1 Quality of SLIP data**

243 Owing to elevated and variable salinity of the coastal water samples from both cores and modern tidal flat are  
244 characterised by low microfauna diversity and low number of foraminifera species. This precludes the use of  
245 transfer function statistics and compels analysis based on direct comparison with the modern environment.

246 We have solved this analytical problem by establishing SLIPs exclusively from basal salt-marsh peat in  
247 transgressive contact and by correcting the data for compaction. This analytical rigor allowed generating  
248 more accurate and more precise SLIP data than those reported by Li et al. (2015) because these earlier SLIP  
249 data are characterised by relatively poor chronological and elevation control (for details see supplement).

250 Notwithstanding SLIP improvement in terms of accuracy and precision, fluctuation of the data exist that can  
251 exceed 1 m (e.g. at 3.9 ka and at 5.2 ka, Fig. 7). Although hard to prove due to lack of data, we believe that  
252 these fluctuations are caused by groundwater extraction which lowers the surface in places.

## 253 5.2 The observed Holocene sea-level rise

254 The SLIPs established indicate two phases of sea-level rise during the Holocene. The first phase occurred in  
255 the early Holocene until ~6.5 ka when the sea level rose from -17 m to -4 m. The second phase occurred from  
256 ~6.5 ka to 2 ka when the sea level rose from -4 m to -2 m. The oldest Holocene shoreline in Bohai Bay is,  
257 situated at -17.2 m at ~9.7 ka cal BP, similar to Tian et al. (2017) who indicate ~-20 m at 9.4 ka cal BP based  
258 on seismic units and drilling cores. Between around 8.8 ka and 7.5 ka cal BP the sea level rose rapidly from -  
259 15.4 m to -7.0 m at a rate of ca 6.4 mm/a. Then, from 7.5 ka to 5.2 ka cal BP the relative sea level rose to -3.6  
260 m at an average rate of 1.9 mm/a and to -1.2 m until 3.8 ka cal BP, before falling to -2.1 m at 2.3 ka cal BP  
261 with an average rising rate of ca. 0.4mm/a from 5.2 to 2.3 ka cal BP. The final phase from 2 ka to today is  
262 constrained by only one SLLP from core Q7 dated to 540 cal BP at ~0.5 m (Table 1). Lithostratigraphic data  
263 (Shang et al., 2016) suggest that surface of the intertidal sediment body remained very close to zero m from  
264 the landward limit of the marine transgression to about 2 km inland from the present shoreline. Further  
265 inland, in borehole ZW15 the surface elevation of the same intertidal sediment body is ~3.0 m lower than in  
266 core Q7 (Figs. 3 and 4) suggesting a rise of sea level in Bohai Bay in the last 1000 years.

## 267 5.3 Observed and predicted Holocene sea level

268 We compare our observational data with GIA models employed in this study and with Bradley et al. (2016;  
269 henceforth denoted as BRAD; see also Table S1) who examined several ice-melting scenarios together with a  
270 range of Earth-model parameters, and validated model outputs using published SLIP data from East China  
271 Sea coast including Bohai Bay.  
272 Figure 7a displays observational data and sea-level predictions generated in this study. It shows that none of  
273 GIA models approximates the observations. The difference ranges between around 14 m at 9 ka and 3 m at  
274 2.5 ka. Bohai Bay's oldest Holocene shoreline (~9.7 ka cal BP) is at -17.2 m (observed), at ca -35 m (ANU)  
275 or at ca -10 m (ICE-X). The BRAD model predicts this shoreline to be at ~-20 m at 10 ka. Our observed  
276 shoreline elevation is similar to Sunda Shelf (ca -15 m; Hanebuth et al., 2011) but different to the islands of  
277 Tahiti (ca -28 m; Bard et al., 2010) and Barbados (ca -25 m; Peltier and Fairbanks, 2006). There are two

278 ways to interpret this: (i) the age of the lowermost SLIP in core Q7 is overestimated due to old carbon  
279 contamination of the dating material or, (ii) the relatively shallow shoreline position in our study area is a  
280 deviation from eustasy due to levering of the broad continental shelf in response to ocean load (e.g., Milne  
281 and Mitrovica, 2008). The similarity to the Sunda Shelf and absence of contamination elsewhere in the  
282 sediment cores suggests indeed that the broad-shelf effect (East China Sea shelf; Fig. 1) causes the shallow  
283 shoreline position. More SLIP data are needed to provide unequivocal evidence for it.

284 While SLIP data suggest a rising rate of  $\sim 0.4$  cm/a during the early Holocene, the GIA models indicate  $\sim 0.5$   
285 cm/a (ICE-X) and  $\sim 0.9$  cm/a (ANU). The ICE-X models approximate the observed early Holocene rising rate  
286 but the timing of this rise is offset by about 2000 years. In the ANU model the early Holocene sea level rises  
287 almost twice as fast as the observed one with an offset of  $\sim 500$  years. Thus, the observed early Holocene sea  
288 level rises slower than the modelled sea level. For the mid-late Holocene SLIP data suggest  $\sim 0.04$  cm/a rising  
289 rate while the GIA models indicate a falling sea level. Predictions obtained from ICE-5G and ICE-6G are  
290 generally relatively similar but deviate from each other in the timing of the mid-Holocene sea-level  
291 highstand. The GIA models, including BRAD, show the highstand (4.6 m -3.4 m; 0.5 m) at 7-6 ka while the  
292 SLIP data remain below modern sea level until 2 ka. The misfit between observed and predicted sea level rise  
293 is in the coastal zone south of Bohai Bay much smaller than in our study area (Fig. S3). This should reflect  
294 the geological structure of the area: our study area belongs to the North China Plain Subsidence Basin (Wang  
295 and Li, 1983), while the south of Bohai Bay lies on the edge of Shandong Upland (Fig. 1b). Thus, the most -  
296 likely explanation for the Bohai Bay misfit is subsidence of the coastal plain. Subsidence is a non-GIA  
297 component and should become evident through the residuals (i.e. the difference between observation and  
298 prediction per unit of time; Fig. 7b). Indeed, we identify linearity of residuals for the period 7-0 ka,  
299 suggesting that subsidence dominates the local sea-level signal after the rise of the eustatic sea level has  
300 slowed down. A subsidence rate of 1.25 mm/a is estimated from the residuals, similar to Wang et al. (2003)  
301 who deduced a rate of  $\sim 1.5$  mm/a from the 400-500 m thick Quaternary sequence in the bay. It is possible  
302 that fluvial sediment supply enhanced the subsidence rate in the Holocene. The Yellow River's annual  
303 discharge into Bohai Bay is estimated to 0.2 Gt until 740AD rising to 1.2 Gt until around 1800 when

304 widespread farming on the loess plateau started increasing the river's sediment load (Best, 2019). Thus, the  
305 sea-level rise in Bohai Bay is in the early Holocene dominated by the eustatic sea-level rise and GIA effects  
306 associated with the broad shelf from Bohai Sea to East China Sea, while in the mid-late Holocene it is  
307 dominated by a combination of tectonic subsidence and fluvial sediment load.

#### 308 **4. Conclusions**

309 Using advanced methods for field survey and identification of accurate and precise sea-level markers, we  
310 have established a new Holocene sea-level history for central Bohai Bay. Our new data are not only different  
311 to previously published data in that they do not show the expected mid-Holocene sea level highstand, but  
312 they are also different to global GIA models. We see a possible broad-shelf effect elevating the shoreline by  
313 several meters in comparison to the tropical islands of Tahiti and Barbados and we see local processes  
314 controlling shoreline migration and coast evolution as soon as ice melting ceased. This indicates that more  
315 emphasis should be placed on regional coast and sea-level change modelling under a global sea-level rising  
316 future as the local government need more specific and effective advice to deal with coastal flooding.

#### 317 **5. ACKNOWLEDGMENTS**

318 We thank one anonymous reviewer and Sarah Bradley for constructive suggestions on the manuscript. This  
319 work was supported by the China Geological Survey, CGS (DD20189506) and National Natural Science  
320 Foundation of China (Grant no. 41476074, 41806109, 41972196). The authors acknowledge PALSEA, a  
321 working group of the International Union for Quaternary Sciences (INQUA) and Past Global Changes  
322 (PAGES), which in turn received support from the Swiss Academy of Sciences and the Chinese Academy of  
323 Science.

#### 324 **References**

325 Amante, C. and Eakins, B.: ETOPO1 Arc-Minute Global Relief Model: Procedures, Data Source and  
326 Analysis. Tech. rep, DOI: 10.7289/V5C8276M, 2009.

- 327 Bard, E., Hamelin, B. and Delanghe-Sabatier, D.: Deglacial meltwater pulse 1B and Younger Dryas sea  
328 levels revisited with boreholes at Tahiti. *Science*, 327, 1235–1237. DOI: 10.1126/science.1180557, 2010.
- 329 Best, J.: Anthropogenic stresses on the world's big rivers. *Nature Geoscience*, 12, 7–21.  
330 Doi:10.1038/s41561-018-0262-x, 2019.
- 331 Bradley, S.L., Milne, G.A., Horton, B.P., Zong, Y.Q.: Modelling sea level data from China and Malay-  
332 Thailand to estimate Holocene ice-volume equivalent sea level change. *Quaternary Science Reviews*, 137,  
333 54–68. DOI: 10.1016/j.quascirev.2016.02.002, 2016.
- 334 Brain, M.J. Chapter 30 Compaction. In: Shennan, I., Long, A.J., Horton, B.P. (Eds.): *Handbook of Sea-level*  
335 *Research*. John Wiley & Sons Ltd. Chichester, UK, 2015.
- 336 Cang, S.X., Zhao, S.L., Zhang, H.C., Huang, Q.F.: Middle Pleistocene paleoecology, paleoclimatology and  
337 paleogeography of the western coast of Bohai Gulf. *Acta Palaeontologica Sinica* 18(6): 579–591. DOI:  
338 10.19800/j.cnki.aps.1979.06.006, 1979 (in Chinese with English abstract).
- 339 Farrell, W. and Clark, J.: On postglacial sea-level. *Geophys. J. Roy. Astr. S.*, 46, 647–667. DOI:  
340 10.1111/j.1365-246X.1976.tb01252.x, 1976
- 341 Feng, X.L., Lin, L., Zhuang, Z.Y, Pan, S.C.: The relationship between geotechnical parameters and  
342 sedimentary environment of soil layers since Holocene in modern Huanghe subaqueous Delta. *Coastal*  
343 *Engineering*, 18, 4, 1–7. DOI: CNKI:SUN:HAGC.0.1999-04-000, 1999 (in Chinese with English abstract).
- 344 Geng, X.S.: Marine transgressions and regressions in east China since late Pleistocene Epoch. *Acta*  
345 *Oceanologica Sinica*, 3(1), 114–130.  
346 [http://www.hyxb.org.cn/aos/ch/reader/create\\_pdf.aspx?file\\_no=19810110&flag=&journal\\_id=aos&year\\_id](http://www.hyxb.org.cn/aos/ch/reader/create_pdf.aspx?file_no=19810110&flag=&journal_id=aos&year_id)  
347 =1981, 1981 (in Chinese with English abstract).
- 348 Hanebuth, T.J.J., Voris, H.K., Yokoyama, Y., Saito, Y., Okuno, J.I.: Formation and fate of sedimentary  
349 depocentres on Southeast Asia's Sunda Shelf over the past sea-level cycle and biogeographic implications.  
350 *Earth-Science Reviews*, 104(1–3), 92–110. <https://doi.org/10.1016/j.earscirev.2010.09.006>, 2011.
- 351 He, Q.X.(Eds.): *Marine Sedimentary Geology of China*. Beijing: China Ocean Press: 464–466, 2006 (in  
352 Chinese).

- 353 IPCC: Climate Change 2014: Synthesis Report. Contribution of Working Groups I, II and III to the Fifth  
354 Assessment Report of the Intergovernmental Panel on Climate Change [Core Writing Team, R.K. Pachauri  
355 and L.A. Meyer (eds.)]. IPCC, Geneva, Switzerland, 151 pp. <https://www.ipcc.ch/report/ar5/syr/>, 2014.
- 356 Lambeck, K., Purcell, A., Johnston, P., Nakada, M., Yokoyama, Y.: Water-load definition in the glacio-  
357 hydro-isostatic sea-level equation. *Quaternary Science Reviews*, 137, 54–68. DOI: 10.1016/s0277-  
358 3791(02)00142–7, 2003.
- 359 Li, J.F.; Kang, H.; Wang, H.; Pei, Y.D.; Modern geological action and discussion of influence factors on the  
360 west coast of Bohai Bay, China. *Geological Survey and Research*, 30(4), 295–301.  
361 <http://www.tianjin.cgs.gov.cn/dzdcyyj/qkxz/20074/200801/P020160920812081540884.pdf>, 2007 (in  
362 Chinese with English abstract).
- 363 Li, J., Pei, Y., Wang, F., Wang, H.: Distribution and environmental significance of living foraminiferal  
364 assemblages and taphocoenose in Tianjin intertidal zone, the west coast of Bohai Bay. *Marine geology &*  
365 *Quaternary geology*, 29(3), 9–21. DOI: CNKI:SUN:HYDZ.0.2009-03-004, 2009. (in Chinese with English  
366 abstract).
- 367 Li, J., Shang, Z., Wang, F., Chen, Y., Tian, L., Jiang, X., Wang, H.: Holocene sea level change on the west  
368 coast of the Bohai Bay. *Quaternary Sciences*, 35(2), 243–264. DOI: 10.11928/j.issn.1001-  
369 7410.2015.02.01, 2015 (in Chinese with English abstract).
- 370 Li, S.L.: Distribution of the foraminiferal thanatocoenosis of PEARL River estuary. *Marine geology &*  
371 *Quaternary Geology*, 5(2), 83–101. DOI: 10.16562/j.cnki.0256-1492.1985.02.009, 1985 (in Chinese with  
372 English abstract).
- 373 Milne, G.A. and Mitrovica J.X.: Searching for eustasy in deglacial sea-level histories. *Quaternary Science*  
374 *Reviews*, 27, 2292–2302. DOI: 10.1016/j.quascirev.2008.08.018, 2008. Mitrovica, J. and Wahr, J.: Ice Age  
375 Earth Rotation. *Annual Review of Earth and Planetary Sciences*, 39, 577–616. DOI: 10.1146/annurev-  
376 earth-040610-133404, 2011.
- 377 Nakada, M. and Lambeck, K.: Glacial rebound and relative sea-level variations: a new appraisal.  
378 *Geophysical Journal International*, 90, 1, 171–224. DOI: 10.1111/j.1365-246X.1987.tb00680.x, 1987.



- 379 Nicholls, R.J. and Cazenave A.: Sea-level rise and its impact on coastal zones. *Science*, 328, 1517–1520.  
380 DOI: 10.1126/science.1185782, 2010.
- 381 Peltier, W.R.: Global glacial isostasy and the surface of the ice-age Earth: the ICE-5G (VM2) Model and  
382 GRACE, *Annu. Rev. Earth Pl. Sc.*, 32, 111–149.  
383 <https://doi.org/10.1146/annurev.earth.32.082503.144359>, 2004.
- 384 Peltier, W.R., Drummond, R., and Roy, K.: Comment on Ocean mass from GRACE and glacial isostatic  
385 adjustment by DP Chambers et al., *J. Geophys. Res.-Sol. Ea.*, 117, B11403.  
386 <https://doi.org/10.1029/2011JB008967>, 2012.
- 387 Peltier, W.R., and Fairbanks, R.G.: Global glacial ice volume and Last Glacial Maximum duration from an  
388 extended Barbados sea level record, *Quat. Sci. Rev.*, 25(23), 3322–3337. DOI:  
389 10.1016/j.quascirev.2006.04.010, 2006.
- 390 Qin, L., Shang, Z.W., Li, Y., Li, J.F.: Temporal and spatial distribution of the oyster reef in Biaokou to  
391 Zengkouhe area; *Geological Survey and Research*, 40(4), 306–310.  
392 <http://www.tianjin.cgs.gov.cn/dzdcyyj/qkxz/20174/201802/P020180202566954723921.pdf>, 2017 (in  
393 Chinese with English abstract).
- 394 Reimer, P.J., Bard, E., Bayliss, A., Beck, J.W., Blackwell, P.G., Ramsey, C.B., Buck, C.E., Cheng, H.,  
395 Edwards, R.L., Friedrich, M., Grootes, P.M., Guilderson, T.P., Haflidason, H., Hajdas, I., Hatté, C.,  
396 Heaton, T.J., Hogg, A.G., Hughen, K.A., Kaiser, K.F., Kromer, B., Manning, S.W., Niu, M., Reimer,  
397 R.W., Richards, D.A., Scott, E.M., Southon, J.R., Turney, C.S.M., van der Plicht, J.: IntCal13 and  
398 MARINE13 radiocarbon age calibration curves 0–50000 years cal BP. *Radiocarbon*, 55(4), 1869–1887.  
399 doi: 10.2458/azu\_js\_rc.55.16947Bronk Ramsey C and Lee S (2013), 2013.
- 400 Shang, Z.W., Wang, F., Li, J.F., Marshall, W.A., Chen, Y.S., Jiang, X.Y., Tian, L.Z., Wang, H.: New  
401 residence times of the Holocene reworked shells on the west coast of Bohai Bay, China. *Journal of Asian*  
402 *Earth Sciences*, 115, 492–506. DOI: 10.1016/j.jseaes.2015.10.008, 2016.

- 403 Shang, Z.W., Wang, F., Fang J., Li, J.F., Chen, Y.S., Jiang, X.Y., Tian, L.Z., Wang, H.: Radiocarbon ages of  
404 different fractions of peat on coastal lowland of Bohai Bay: marine influence? *Journal of Oceanology and*  
405 *Limnology*, <https://doi.org/10.1007/s00343-019-7091-7>, 2018.
- 406 Shennan, I., Long, A.J. and Horton, B.P.(Eds.): *Handbook of sea-level research*. Published by John Wiley &  
407 Sons, Ltd., 2015.
- 408 Spada, G. and Stocchi, P.: SELEN: a Fortran 90 program for solving the “Sea Level Equation”, *Comput.*  
409 *Geosci.*, 33, 538–562. DOI: 10.1016/j.cageo.2006.08.006, 2007.
- 410 Spada, G. and Melini, D.: SELEN4 (SELEN version 4.0): a Fortran program for solving the gravitationally  
411 and topographically self-consistent sea-level equation in glacial isostatic adjustment modelling.  
412 *Geoscientific Model Development*, 12, 5055–5075. DOI: 10.5194/gmd-12-5055-2019, 2019
- 413 Su, S.W., Shang, Z.W., Wang, F., Wang, H.: Holocene Chenier: spatial and temporal distribution and sea  
414 level indicators in Bohai Bay. *Geological Bulletin of China*, 30(9), 1382–1395. DOI: 10.1007/s11589-011-  
415 0776-4, 2011(in Chinese with English abstract).
- 416 Tian, L.Z., Chen, Y.P., Jiang, X.Y., Wang, F., Pei, Y.D., Chen, Y.S., Shang, Z.W., Li, J.F., Li, Y., Wang, H.:  
417 Post-glacial sequence and sedimentation in the western Bohai Sea, China. *Marine Geology*, 388m 12–24.  
418 <http://dx.doi.org/10.1016/j.margeo.2017.04.006>, 2017.
- 419 Tegmark, M.: An icosahedron-based method for pixelizing the celestial sphere, *Astrophys. J.*, 470, L81–L85,  
420 <https://doi.org/10.1086/310310>, 1996.
- 421 Wang, F., Li, J.F., Chen, Y.S., Fang, J., Zong, Y.Q., Shang, Z.W., Wang H.: The record of mid-Holocene  
422 maximum landward marine transgression in the west coast of Bohai Bay, China. *Marine Geology*, 359,  
423 89–95. DOI: 10.1016/j.margeo.2014.11.013, 2015.
- 424 Wang, H., Chen, Y.S., Tian, L.Z., Li, J.F., Pei, Y.D., Wang, F., Shang, Z.W., Fan, C.F., Jiang, X.Y., Su,  
425 S.W., Wang, H.: Holocene cheniers and oyster reefs in Bohai Bay: palaeoclimate and sea level changes.  
426 *Geological Bulletin of China*, 30(9), 1405–1411. DOI: 10.1007/s11589-011-0776-4, 2011(in Chinese with  
427 English abstract).

- 428 Wang, P.X., Min, Q.B. and Bian, Y.H.: Distributions of foraminifera and ostracoda in bottom sediments of  
429 the northwestern part of the South Huanghai (Yellow) Sea and its geological significance. In: Wang, P.  
430 (Eds.), *Marine Micropaleontology of China*. China Ocean Press, Beijing, pp. 93–114, 1985 (in Chinese  
431 with English abstract).
- 432 Wang, P.X., Min, Q.B., Bian, Y.H., Cheng, X.R.: Strata of quaternary transgressions in east China: a  
433 preliminary study. *Acta Geologica Sinica*, 1, 1–13. DOI: 10.1007/BF01077538, 1981 (in Chinese with  
434 English abstract).
- 435 Wang, Q. and Li F.L.: The changes of marine-continental conditions in the west coast of the Bohai Gulf  
436 during Quaternary. *Marine Geology&Quaternary Geology*, 4, 83–89. DOI: 10.16562/j.cnki.0256-  
437 1492.1983.04.013, 1983 (in Chinese with English abstract).
- 438 Wang, R.B., Zhou, W., Li, F.L., Wang, H., Yang, G.Y., Yao, Z.J., Kuang, S.J.: Tectonic subsidence and  
439 prospect of ground subsidence control in Tianjin area. *Hydrogeology & Engineering Geology*, 5, 12–17.  
440 DOI: 10.1007/BF02873153, 2003 (in Chinese with English abstract).
- 441 Wang, Y.: The shell coast ridges and the old coastlines of the west coast of the Bohai Bay. *Bulletin of*  
442 *Nanjing University (Edition of Natural Sciences)*, 8(3), 424–440. DOI: CNKI:SUN:NJDZ.0.1964-03-007,  
443 1964 (with three plates) (in Chinese with English abstract).
- 444 Wang, Y.M.: A preliminary study on the Holocene transgression on the coastal plain along the north-western  
445 Bohai Bay. *Geographical Research*, 1(2), 59–69. DOI: 10.11821/yj1982020007, 1982 (in Chinese with  
446 English abstract).
- 447 Wang, Z., Zhuang, C., Staito, Y., Chen, J., Zhan, Q., Wang, X.: Early mid-Holocene sea-level change and  
448 coastal environmental response on the southern Yangtze delta plain, China: implications for the rise of  
449 Neolithic culture. *Quaternary Science Reviews*, 35, 51–62. DOI: 10.1016/j.quascirev.2012.01.005, 2012.
- 450 Wang, Z., Jones, B.G., Chen, T., Zhao, B., Zhan, Q.: A raised OIS3 sea level recorded in coastal sediments,  
451 southern Changjiang delta plain, China. *Quaternary Research*, 79, 424–438. DOI:  
452 10.1016/j.yqres.2013.03.002, 2013.

- 453 Xiong, H., Zong, Y., Qian, P., Huang, G., Fu, S.: Holocene sea-level history of the northern coast of South  
454 China Sea. *Quaternary Science Reviews* 194, 12–26. <https://doi.org/10.1016/j.quascirev.2018.06.022>,  
455 2018.
- 456 Xiong, H., Zong, Y., Li, T., Long, T., Huang, G., Fu, S.: Coastal GIA processes revealed by the early to  
457 middle Holocene sea-level history of east China. *Quaternary Science Reviews*, 233, 106249. DOI:  
458 10.1016/j.quascirev.2020.106249, 2020.
- 459 Xue, C.T.: Historical changes in the Yellow River delta, China. *Marine Geology* 113, 321–329. DOI :  
460 10.1016/0025-3227(93)90025-Q, 1993.
- 461 Yang, H.R. and Chen, Q.X.: Quaternary transgressions, eustatic changes and shifting of shoreline in east  
462 China. *Marine Geology & Quaternary Geology*, 5(4), 69–80. DOI: 10.16562/j.cnki.0256-  
463 1492.1985.04.011, 1985 (in Chinese with English abstract).
- 464 Zhang, Y.C., Hu, J.J. and Liu, C.F.: Preliminary recognition of sea and land changes along the east coast of  
465 China since the terminal Pleistocene. *Bulletin of the Chinese Academy of Geological Sciences*, 19, 37–52.  
466 <https://www.ixueshu.com/document/8e1a59a8c6fd86ca318947a18e7f9386.html>, 1989 (in Chinese with  
467 English abstract).
- 468 Zhao, S.L., Yang, G.F., Cang, S.X., Zhang, H.C., Huang, Q.F., Xia, D.X., Wang, Y.J., Liu, F.S., Liu, C.F.:  
469 On the marine stratigraphy and coastlines of the western coast of the gulf of Bohai. *Oceanologia Et*  
470 *Limnologia Sinica*, 9(1), 15–25  
471 [http://qdhs.ijournal.cn/hyyhz/ch/reader/create\\_pdf.aspx?file\\_no=19780102&flag=&journal\\_id=hyyhz&ye](http://qdhs.ijournal.cn/hyyhz/ch/reader/create_pdf.aspx?file_no=19780102&flag=&journal_id=hyyhz&ye)  
472 [ar\\_id=1978](http://qdhs.ijournal.cn/hyyhz/ch/reader/create_pdf.aspx?file_no=19780102&flag=&journal_id=hyyhz&year_id=1978), 1978 (in Chinese with English abstract).
- 473 Zhao, X.T., Geng, X.S., Zhang, J.W.: Sea level changes of the eastern China during the past 20000 years.  
474 *Acta Oceanologia Sinica*, 1(2), 269–281.  
475 [http://www.hyxb.org.cn/aos/ch/reader/create\\_pdf.aspx?file\\_no=19790208&year\\_id=1979&quarter\\_id=2&f](http://www.hyxb.org.cn/aos/ch/reader/create_pdf.aspx?file_no=19790208&year_id=1979&quarter_id=2&f)  
476 [alg=1](http://www.hyxb.org.cn/aos/ch/reader/create_pdf.aspx?file_no=19790208&year_id=1979&quarter_id=2&file_id=1), 1979.
- 477 Zong, Y.: Mid-Holocene sea-level highstand along the southeast coast of China. *Quaternary International*,  
478 117, 55–67. DOI: 10.1016/S1040-6128(03)00116-2, 2004.

479

**Table 1. Analytical data used to establish SLIPs.**

Beta-lab code	Depth (m)	Altitude (m, msl)	Dated material	$\delta^{13}\text{C}$ (‰)	Conventional age (BP)	Calibrated age (BP) ( $2\sigma$ )	Median age (BP)	Indicative meaning and range	Sediment compaction (m)*	Palaeo-mean sea level
<b>Core DC01</b>										
329636	8.40	-4.66	Peat	-26.8	6950±40	7523-7430	7487	Terrestrial peat		
329637	9.27	-5.53	Bulk organic	-18.2	7410±60	8372-8153	8248	Terrestrial peat		
<b>Core QX01</b>										
329647	5.52	+0.36	Bulk organic	-22.5	4300±30	4892-4829	4343**	1.78±0.53	0.29±0.04	-1.14±0.57
329644	6.35	-1.19	Bulk organic	-23.6	5010±50	5900-5644	5226**	1.78±0.53	0.30±0.04	-2.68±0.57
329643	7.20	-2.04	Bulk organic	-25.0	5090±30	5912-5748	5288**	1.78±0.53	0.25±0.03	-3.58±0.56
329641	8.20	-3.04	Peat	-24.6	5830±30	6732-6554	6647	1.78±0.53	0.24±0.03	-4.58±0.56
329642	8.70	-3.54	Peat	-24.3	6030±40	6981-6778	6875	1.78±0.53	0.21±0.03	-5.11±0.56
329645	9.16	-4.00	Peat	-27.4	6220±40	7250-7006	7117	1.78±0.53	0.18±0.02	-5.60±0.55
329640	11.39	-6.23	Peat	-25.3	7010±30	7935-7786	7855	1.78±0.53	0.01±0.01	-8.00±0.54
329646	13.05	-7.89	Peat	-25.1	7200±30	8057-7952	8002	Terrestrial peat		
<b>Core QX03</b>										
353792	2.91	1.47	Peat	-20.6	2350±30	2461-2326	2357	Terrestrial peat		
353794	4.90	-0.42	Peat	-24.0	3390±30	3699-3569	3634	1.78±0.53	0.16±0.02	-2.01±0.55
353796	7.39	-3.01	Plant material	NA	5930±30	6799-6671	6752	1.78±0.53	0.10±0.02	-4.68±0.55
353798	8.63	-4.25	Plant material	-26.7	6410±40	7420-7271	7350	1.78±0.53	0.01±0.01	-6.02±0.54
353800	9.60	-5.22	Plant material	-28.2	6690±40	7622-7478	7562	Terrestrial peat		
353802	12.40	-8.02	Plant material	-28.3	7280±40	8429-8325	8397	Terrestrial peat		
<b>Core QX02</b>										

332798	3.65	-0.08	Bulk organic	-23.6	3680±30	4091-3913	3517**	1.78±0.53	0.30±0.04	-1.57±0.57
332792	5.68	-2.11	Bulk organic	-24.0	5450±30	6300-6204	5718**	1.78±0.53	0.36±0.04	-3.54±0.57
333329	7.27	-3.70	Peat	-26.7	6350±30	7331-7240	7283	1.78±0.53	0.32±0.04	-5.16±0.57
333330	8.98	-5.41	Peat	-26.3	6600±30	7522-7434	7494	1.78±0.53	0.19±0.02	-7.00±0.55
333331	10.97	-7.40	Peat	-27.2	7020±30	7934-7792	7867	Terrestrial peat		
333333	12.42	-8.85	Peat	-26.3	7140±40	8023-7925	7966	Terrestrial peat		
<b>Core ZW15</b>										
255821	1.6	0.03	Bulk organic	-22.5	2930±30	3168-2976	2584**	1.78±0.53	0.32±0.04	-1.44±0.57
356208	12.6	-10.97	Plant material	-25.0	7450±40	8358-8186	8271	1.78±0.53	0.00	-12.75±0.53
356209	13.5	-11.87	Plant material	-25.5	7640±40	8521-8381	8430	Terrestrial peat		
<b>Core Q7</b>										
358054	1.3	2.16	Bulk organic	-20.4	530±30	559-510	540	1.78±0.53	0.10±0.02	+0.49±0.55
357153	17.2	-13.74	Plant material	-28.0	7990±40	9005-8705	8868	1.78±0.53	0.16±0.02	-15.36±0.55
357157	18.85	-15.39	Bulk organic	-24.6	9140±40	10411-10226	9718**	1.78±0.53	0.00	-17.18±0.53
<b>Core CZ01</b>										
395014	15.42	-8.53	Peat	-27.5	8930±40	10099-9914	10047	Terrestrial peat		
<b>Core CZ02</b>										
395022	12.19	-6.42	Peat	-23.1	7950±30	8980-8648	8830	Terrestrial peat		
<b>Core CZ03</b>										
395026	4.42	-0.48	Bulk organic	-24.2	2730±30	2877-2762	2325**	1.78±0.53	0.12±0.02	-2.15±0.55
395027	6.15	-2.21	Peat	-25.1	4790±30	5593-5470	5517	1.78±0.53	0.19±0.02	-3.80±0.55
395028	6.54	-2.57	Bulk organic	-27.1	5830±30	6732-6554	6114**	1.78±0.53	0.18±0.03	-4.18±0.56
395029	7.51	-3.54	Peat	-26.7	6230±30	7251-7019	7167	1.78±0.53	0.14±0.02	-5.19±0.55
395030	9.22	-5.25	Peat	-27.3	6640±30	7576-7468	7528	1.78±0.53	0.01±0.01	-7.03±0.54

395031	9.34	-5.37	Peat	-20.0	6660±30	7583-7483	7535	1.78±0.53	0.00	-7.15±0.53
395032	10.23	-6.26	Peat	-27.2	6900±30	7794-7669	7726	Terrestrial peat		
395034	12.4	-8.43	Peat	-27.2	7290±30	8171-8025	8102	Terrestrial peat		
<b>Core CZ87</b>										
403413	2.66	1.8	Bulk organic	-20.8	2420±30	2696-2351	2446	Terrestrial peat		
403414	4.51	-0.05	Bulk organic	-23.8	3330±30	3637-3477	3566	Terrestrial peat		
406826	5.75	-1.29	Bulk organic	-24.1	4020±30	4536-4420	3970**	1.78±0.53	0.25±0.03	-2.83±0.56
403417	11.05	-6.59	Plant material	-27.9	6300±30	7275-7165	7223	1.78±0.53	0.04±0.01	-8.33±0.54
403418	12.62	-8.16	Plant material	-27.6	6990±30	7876-7736	7829	Terrestrial peat		
<b>Core CZ61</b>										
407339	2.52	1.24	Bulk organic	-20.8	2310±30	2359-2306	2337	Terrestrial peat		
406823	4.72	-0.96	Plant material	NA	2780±30	2952-2793	2877	1.78±0.53	0.16±0.02	-2.58±0.55
406824	6.20	-2.44	Bulk organic	-23.9	6100±30	7029-6884	6433**	1.78±0.53	0.25±0.03	-3.98±0.56
403397	9.73	-5.97	Plant material	-19.6	6760±30	7664-7577	7615	1.78±0.53	0.00	-7.75±0.53
403398	11.04	-7.37	Plant material	-27.5	7000±30	7932-7756	7842	Terrestrial peat		
403399	12.90	-9.14	Plant material	-28.0	7160±30	8018-7939	7980	Terrestrial peat		
<b>Core CZ65</b>										
399705	4.93	-1.97	Bulk organic	-18.5	3920±30	4428-4280	3397	Terrestrial peat		
399708	9.58	-6.62	Plant material	-27.2	7000±30	7883-7756	7823	1.78±0.53	0.01±0.01	-8.39±0.54
399710	11.50	-8.54	Plant material	-27.1	7250±30	8162-8001	8080	Terrestrial peat		
<b>Core CZ80</b>										
403401	3.73	2.69	Bulk organic	-20.3	3170±30	3452-3346	3400	Terrestrial peat		
403403	6.57	-0.15	Bulk organic	-22.1	5050±30	5901-5726	5298	1.78±0.53	0.20±0.03	-1.74±0.56
406825	8.75	-2.33	Peat	NA	5840±30	6736-6562	6660	1.78±0.53	0.09±0.01	-4.02±0.54

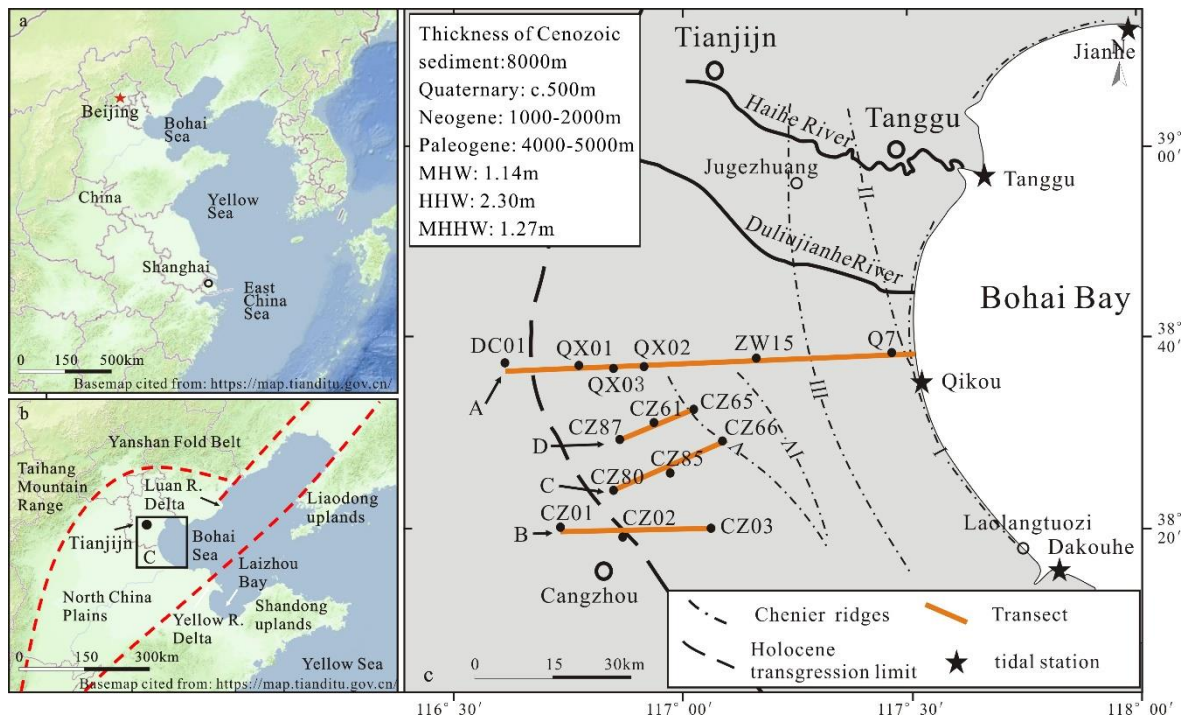
403408	11.53	-5.11	Plant material	-27.5	6450±30	7428-7313	7370	Terrestrial peat		
403409	12.05	-5.63	Plant material	-27.9	6610±30	7565-7440	7503	Terrestrial peat		
403410	12.34	-5.92	Plant material	-26.4	6860±30	7759-7618	7687	Terrestrial peat		
403411	13.84	-7.42	Plant material	-24.6	7300±30	8175-8029	8105	Terrestrial peat		
<b>Core CZ85</b>										
399719	3.67	0.94	Bulk organic	-20.5	3460±30	3671-3641	3225**	1.78±0.53	0.17±0.03	-0.68±0.56
399720	6.77	-2.16	Bulk organic	-25.4	5830±30	6732-6554	6114**	1.78±0.53	0.08±0.01	-3.87±0.54
399721	8.33	-3.72	Plant material	-26.4	6020±30	6947-6785	6862	1.78±0.53	0.01±0.01	-5.49±0.54
399722	12.70	-8.09	Plant material	-28.0	7270±30	8165-8015	8096	Terrestrial peat		
<b>Core CZ66</b>										
399712	3.62	0.25	Bulk organic	-23.4	3930±30	4440-4282	3856**	1.78±0.53	0.32±0.04	-1.22±0.57
399713	5.21	-1.34	Bulk organic	-25.1	5730±30	6632-6445	5992**	1.78±0.53	0.39±0.05	-2.74±0.58
399714	8.14	-4.27	Plant material	-27.4	6710±30	7651-7510	7581	1.78±0.53	0.24±0.03	-5.81±0.56
399715	10.03	-6.16	Plant material	-26.6	6790±30	7675-7587	7635	1.78±0.53	0.08±0.01	-7.86±0.54
399716	12.49	-8.62	Plant material	-27.1	7220±30	8156-7965	8021	Terrestrial peat		
399718	13.63	-9.76	Plant material	-27.6	7670±30	8523-8406	8452	Terrestrial peat		

480 s\* Sediment compaction = 10% of compressible thickness divided by lapse time of deposition in the past 9000 years

481 \*\* corrected for marine influence on salt marsh organic sample fraction ages of peaty clay

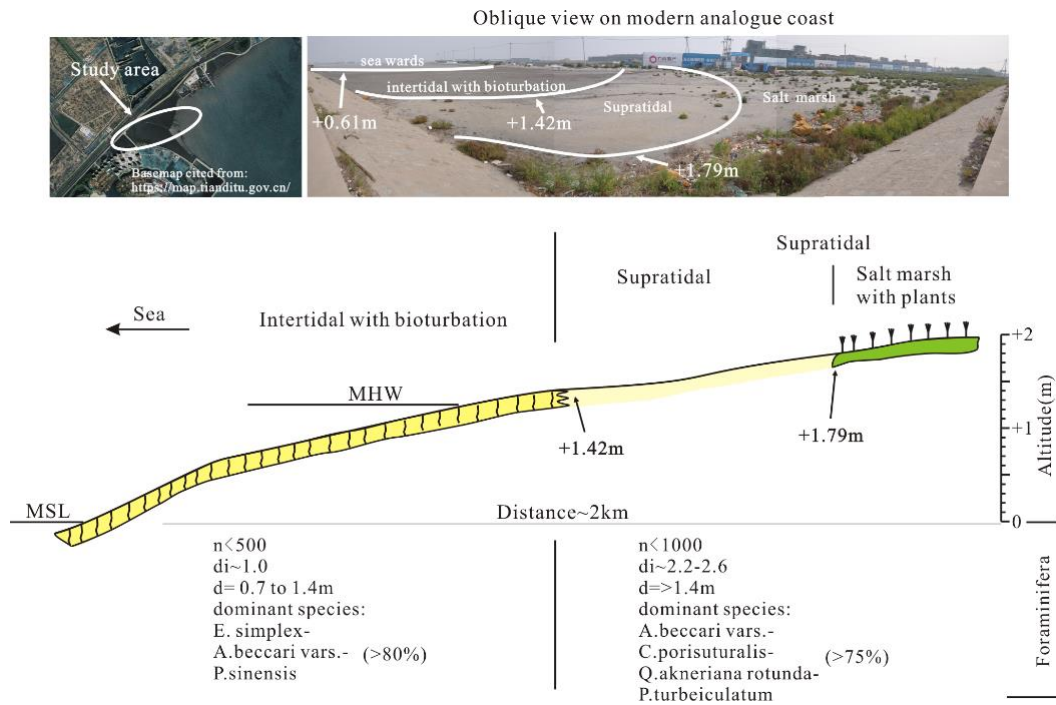
482



483 **Figure captions**

484

485 **Figure 1. The study area; (a) location of Bohai Bay and Yellow Sea; (b) location of the study area and major river**486 **deltas; red dashed lines indicate the topographic boundaries of coastal lowland, (c) locations of boreholes,**487 **transects A, B, C, D, Chenier ridges (Su et al. (2011; Wang et al., 2011) and Holocene transgression limit (Xue,**488 **1993). The basemap of Fig.1a and Fig.1b are cited from "map world" (<https://www.tianditu.gov.cn/>, National**489 **Platform for Common Geispatial Information Services, China)**

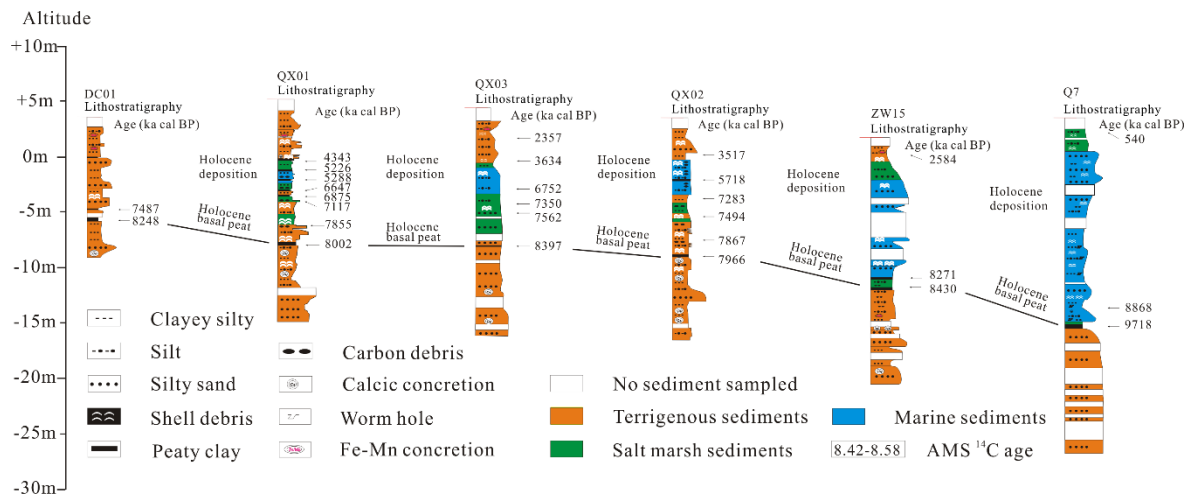


490

491 **Figure 2. Schematic cross-section of the modern tidal flat of the study area showing two characteristic**

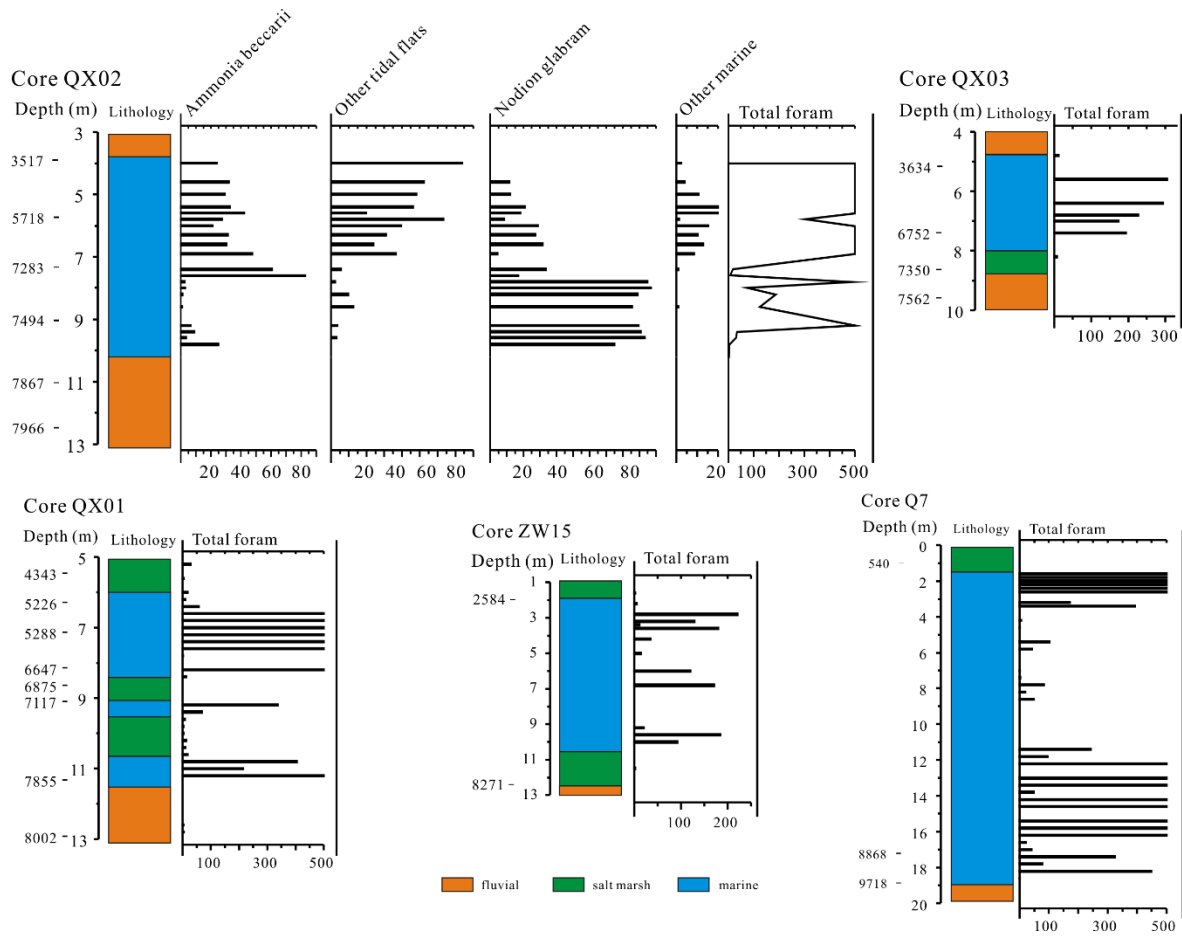
492 **foraminiferal zones. The basemap of study area is derived from "map world" (<https://www.tianditu.gov.cn/>,**

493 **National Platform for Common Geospatial Information Services, China)**



494

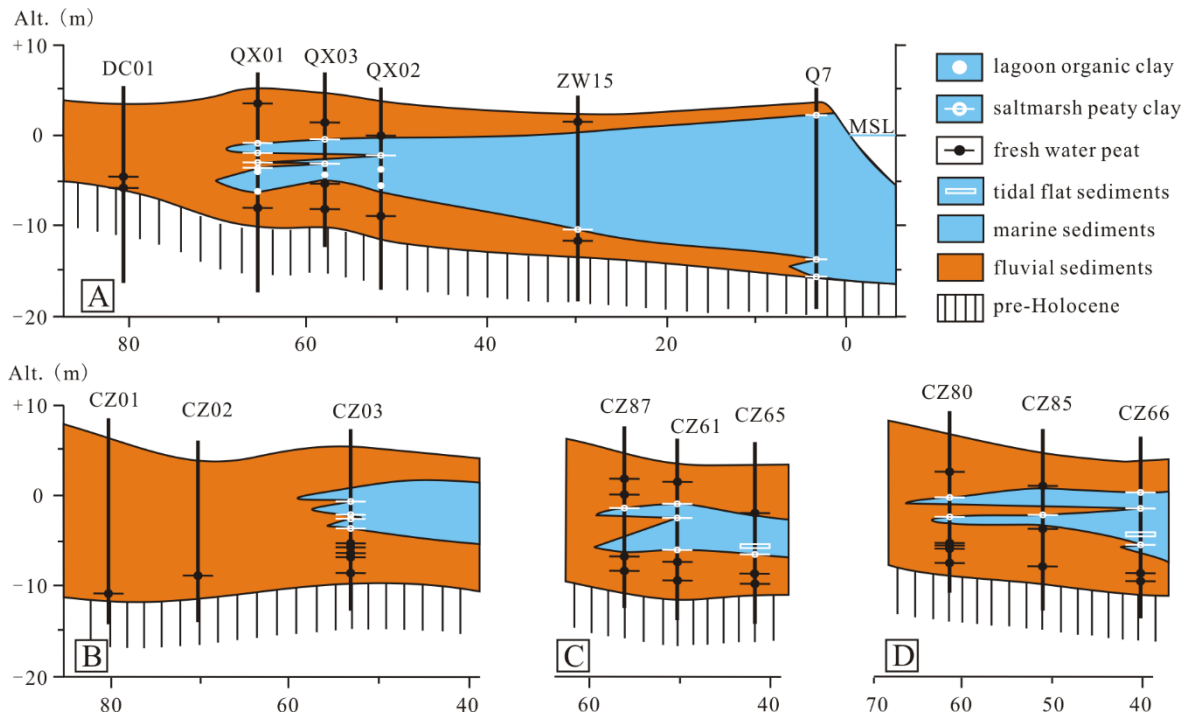
495 **Figure 3. The lithostratigraphy of transect A, with details of dated sedimentary horizons.**



496

497

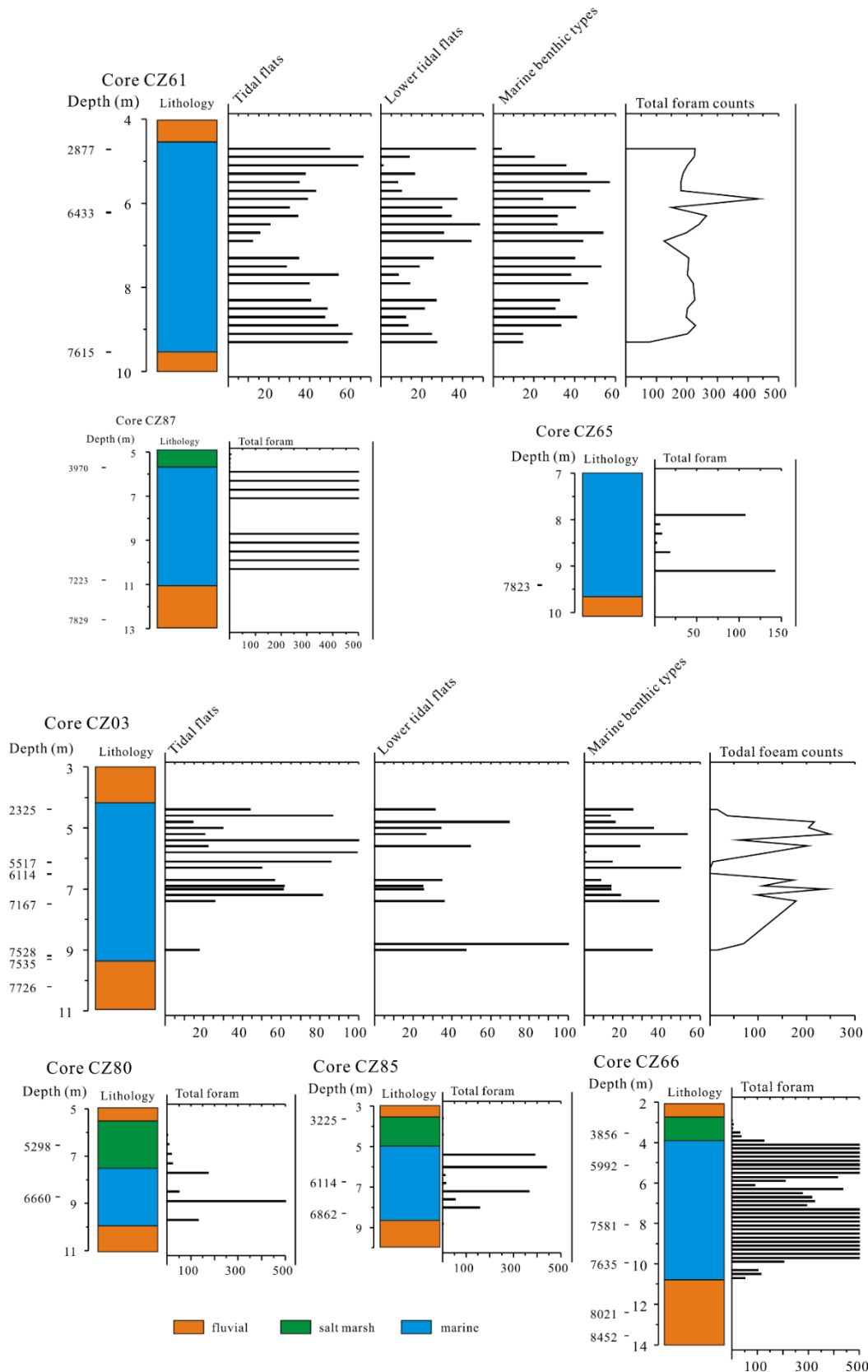
Figure 4. Foraminiferal counts from five cores of transect A. Counts > 500 are shown as 500.



498

499

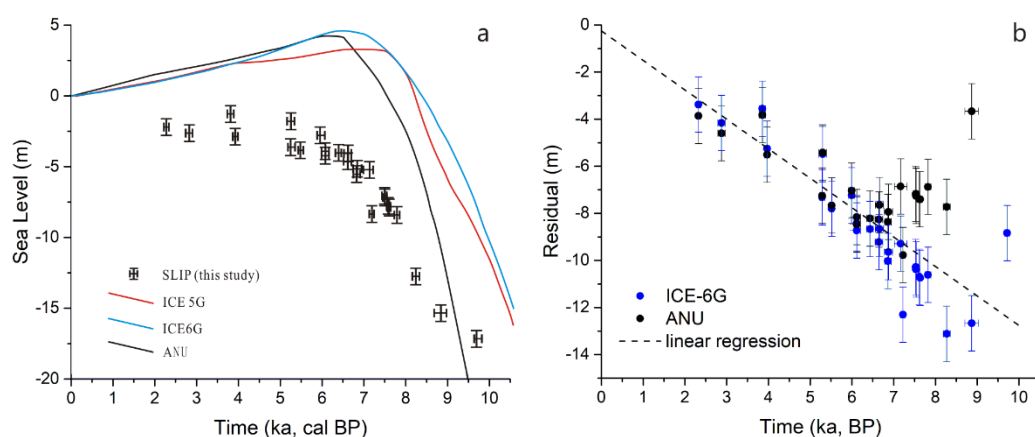
Figure 5. The lithostratigraphy of transects B, C and D, with details of dated sedimentary horizons.



500

501 **Figure 6. Foraminiferal counts from five cores of transects B, C and D. Counts > 500 foraminifera are shown as**

502 **500.**



503

504 **Figure 7. Observed and predicted sea level in Bohai Bay and resulting residuals; (a) SLIPs generated in this study**505 **and sea-level predictions. ICE-5G, ICE-6G and ANU are GIA models described in section 3.6. Lithospheric**506 **thickness (km): 65 (ANU), 90 (5G and 6G); upper mantle viscosity (Pa s) =  $0.5 \times 10^{21}$  (ANU, 5G, 6G); lower mantle**507 **viscosity (Pa s):  $10 \times 10^{21}$  (ANU),  $2.7 \times 10^{21}$  (5G),  $3.2 \times 10^{21}$  (6G); see also Table S1; age error bars are too small to be**508 **clearly visible. (b) Sea-level residuals plotted against time. Residuals are the difference between SLIPs and**509 **interpolated model data points. Error bars are derived from SLIP uncertainties. The trend line (dashed line) is**510 **computed as a least-squares regression on the mean residuals obtained with ANU and ICE-6G. The regression line**511 **approximates zero elevation remarkably closely which gives confidence that the calculated 1.25 mm/a for the non-**512 **GIA component is correct.**

513

## 514 Author contribution

Author name	Contributions
Fu Wang	Scientific questions choice, design of field work including sampling and measurements, data analyses, results and discussion, paper writing and revising.
Yongqiang Zong	Revise part of the paper and English writing check.
Barbara Mauz	Revise part of the paper and English writing check.
Jianfen Li	Sampling and foraminifera analysis.
Jing Fang	Sampling and foraminifera analysis.
Lizhu Tian	Sampling and foraminifera analysis.
Yongsheng Chen	Sampling and foraminifera analysis.
Zhiwen Shang	Sampling and foraminifera analysis.
Xingyu Jiang	Sampling and foraminifera analysis.
Giorgio Spada	GIA model work and writing sec 3.6
Daniele Melini	GIA model work and residual calculation

515